Investigating changes in axonal density and morphology of glaucomatous optic nerves using fixel-based analysis

Haykal, Shereif; Jansonius, Nomdo M; Cornelissen, Frans W

Published in:
European Journal of Radiology

DOI:
10.1016/j.ejrad.2020.109356

Publication date:
2020

European Journal of Radiology 133 (2020) 109356

Contents lists available at ScienceDirect

European Journal of Radiology

journal homepage: www.elsevier.com/locate/ejrad

Research article

Investigating changes in axonal density and morphology of glaucomatous optic nerves using fixel-based analysis

Shereif Haykal [a,*], Nomdo M. Jansonius [b], Frans W. Cornelissen [a]

[a] Laboratory for Experimental Ophthalmology, University of Groningen, University Medical Center Groningen, Groningen, the Netherlands
[b] Department of Ophthalmology, University of Groningen, University Medical Center Groningen, Groningen, the Netherlands

ARTICLE INFO

Keywords:
Glaucoma
Optic nerve
Magnetic resonance imaging
Diffusion-weighted imaging
Diffusion tensor imaging
Fixel-based analysis

ABSTRACT

Purpose: To characterize neurodegeneration of glaucomatous optic nerves (ONs) in terms of changes in axonal density and morphology using fixel-based analysis (FBA), a novel framework for analyzing diffusion-weighted MRI (DWI). Furthermore, we aimed to explore the potential of FBA measures as biomarkers of glaucomatous ON degeneration.

Methods: DWI scans were obtained from 15 glaucoma patients and 15 controls. ONs were tracked and segmented into their three anatomical segments; intraorbital (IO), intracanalicular (ICAN) and intracranial (ICRAN). For each segment, FBA measures were computed, which included fiber density (FD; a measure of axonal density), fiber-bundle cross-section (FC; an estimate of morphological changes), and fiber density and cross-section (FDC). Peripapillary retinal nerve fiber layer (pRNFL) thickness and visual field mean deviation (VFMD) were assessed for glaucoma patients. ANCOVA was used to compare FBA values between the two groups, and Spearman's correlation analysis was used to test the correlation between FBA measures and pRNFL thickness and VFMD.

Results: All glaucomatous ON segments showed a significant loss of FD and FDC compared to the controls, while a loss of FC was found in the IO and ICRAN segments only. FD and FDC values of the IO and ICAN segments of glaucomatous ONs showed significant correlations with pRNFL thickness and VFMD.

Conclusions: Glaucomatous ONs exhibit lower FD and FC compared to controls, indicating axonal loss and gross atrophy. The correlation between FBA measures of glaucomatous ONs and established clinical tests of glaucoma demonstrates the potential of FBA measures as biomarkers of glaucomatous ON degeneration.

1. Introduction

Glaucoma is a progressive, irreversible optic neuropathy, characterized by the death of retinal ganglion cells (RGCs) and a distinct pattern of visual field loss [1]. Clinical evaluation of glaucoma involves the assessment of both functional loss and structural retinal degeneration. A hallmark of glaucomatous structural degeneration is the loss of retinal nerve fiber layer (RNFL) thickness. The RNFL is composed of RGCs axons, and therefore exhibits a decrease in thickness following the loss of RGCs due to glaucoma.

Glaucomatous structural loss, however, is not confined to the RNFL, but it rather manifests throughout the entire length of the optic nerve (ON) [2], as the ON is primarily formed of myelinated RGC axons. Therefore, probing the ON in glaucoma patients could present a new approach for detecting glaucomatous structural degeneration. Indeed, diffusion-weighted MRI (DWI) studies of glaucoma patients have reported degenerative changes in glaucomatous ONs beyond the retina [3–12]. Furthermore, DWI measures of glaucomatous ONs were found to correlate with ophthalmic measures of glaucoma, indicating the potential of DWI measures as biomarkers of structural glaucomatous

Abbreviations: DWI, diffusion-weighted imaging; FA, fractional anisotropy; FBA, fixel-based analysis; FC, fiber-bundle cross-section; FD, fiber density; FDC, fiber density and cross-section; FDT, frequency doubling technology; FOD, fiber orientation distribution; H-P-A, Hodapp-Parrish-Anderson; HFA, Humphrey field analyzer; ICAN, Intracanalicular; ICRAN, intracranial; IO, intraorbital; IOP, intraocular pressure; MD, mean diffusivity; OCT, optical coherence tomography; ON, optic nerve; OT, optic tract; PEX, pseudoexfoliative glaucoma; POAG, primary open-angle glaucoma; pRNFL, peripapillary retinal nerve fiber layer; RGC, retinal ganglion cell; RNFL, retinal nerve fiber layer; ROI, region of interest; SITA, Swedish interactive threshold algorithm; TE, echo time; TR, repetition time; VFMD, visual field mean deviation; WM, white matter.

* Corresponding author at: Laboratory for Experimental Ophthalmology, University Medical Center Groningen, P.O.Box 30.001, 9700 RB, Groningen, the Netherlands.
E-mail address: s.a.m.m.haykal@umcg.nl (S. Haykal).

https://doi.org/10.1016/j.ejrad.2020.109356
Received 8 June 2020; Received in revised form 18 September 2020; Accepted 11 October 2020
Available online 16 October 2020

degeneration.

To date, most DWI studies of glaucomatous ONs have relied on diffusion tensor imaging (DTI) for data analysis. DTI uses a tensor model to characterize water diffusion on a voxel level, producing measures of white matter (WM) structural integrity such as fractional anisotropy (FA) and mean diffusivity (MD) [13]. However, such DTI measures are nonspecific, as they reflect a wide range of WM structural changes. For example, a change in FA could be a response to changes in membrane permeability, myelination, axonal size or axonal packing density [14]. Furthermore, due to its single-compartmental nature, the tensor model is incapable of distinguishing different tissue types within the same voxel [15]. This can affect the reliability of tensor-derived measures, especially in relatively small structures such as the ON, where partial volume effects from surrounding tissues are inevitable. Therefore, adopting higher-order models which overcome some of the limitations of DTI could improve the prospects of DWI measures as biomarkers of glaucomatous degeneration.

Fixel-based analysis (FBA) is a novel framework for analyzing DWI, which overcomes some of the limitations of DTI by using a multi-compartmental model to analyze distinct WM fiber populations within a voxel (termed "*fixels*") [16]. By doing so, FBA is able to produce measures that directly correspond to biological changes occurring in WM fibers (Fig. 1). These measures are (1) fiber density (FD), (2) fiber-bundle cross-section (FC), and (3) fiber density and cross-section (FDC). FD examines microstructural WM changes by estimating the axonal density of a specific WM fiber population within a voxel [17]. A decrease in FD indicates axonal loss in a WM fiber population. FC, on the other hand, represents morphological (or macrostructural) changes to the cross-sectional area of a specific fiber bundle. A decrease of FC indicates gross atrophy of a WM fiber bundle. Finally, FDC combines FD and FC, providing a more comprehensive measure of the overall information carrying capacity of WM fiber bundles. Thus, characterizing glaucomatous ON degeneration using FBA could provide new insights into the nature of the glaucomatous neurodegeneration and potentially provide reliable biomarkers for clinically assessing the ON of glaucoma patients.

In this study, we aimed to characterize glaucomatous WM degeneration along the different anatomical segments of the ON using FBA. Furthermore, we aimed to evaluate the potential of FBA measures as biomarkers for glaucomatous ON degeneration by determining their correlation with established ophthalmic tests of glaucoma. Finally, for comparison, we performed the same analyses using the conventional voxel-based DTI approach.

2. Methods

2.1. Ethical approval

This study was approved by the ethics board of the University Medical Center Groningen (UMCG). The study adhered to the tenets of the Declaration of Helsinki. All participants provided written informed consent prior to participation.

2.2. Participants

Eighteen glaucoma patients and 18 control subjects were initially recruited for this cross-sectional study. Inclusion criteria for glaucoma patients was having been diagnosed with glaucoma in at least one eye. Inclusion criteria for controls included having an intraocular pressure (IOP) of $\leq$ 21 mmHg, no visual field defects, and a visual acuity of 0.8 or higher (+0.1 logMAR or less) in both eyes. Exclusion criteria for controls and glaucoma patients included having any ophthalmic disease that affects optic nerve structure or function (apart from glaucoma in the glaucoma group), having a neurodegenerative disorder, having an unsuccessful eye exam or MRI scan during data collection, having a contraindication to being inside an MRI scanner, and the detection of any apparent pathology on an acquired MRI scan. Two controls were excluded for having uncorrectable MRI artifacts compromising their DWI scans. Three glaucoma patients were excluded, all for having incomplete eye exams. In total, 15 glaucoma patients and 15 controls

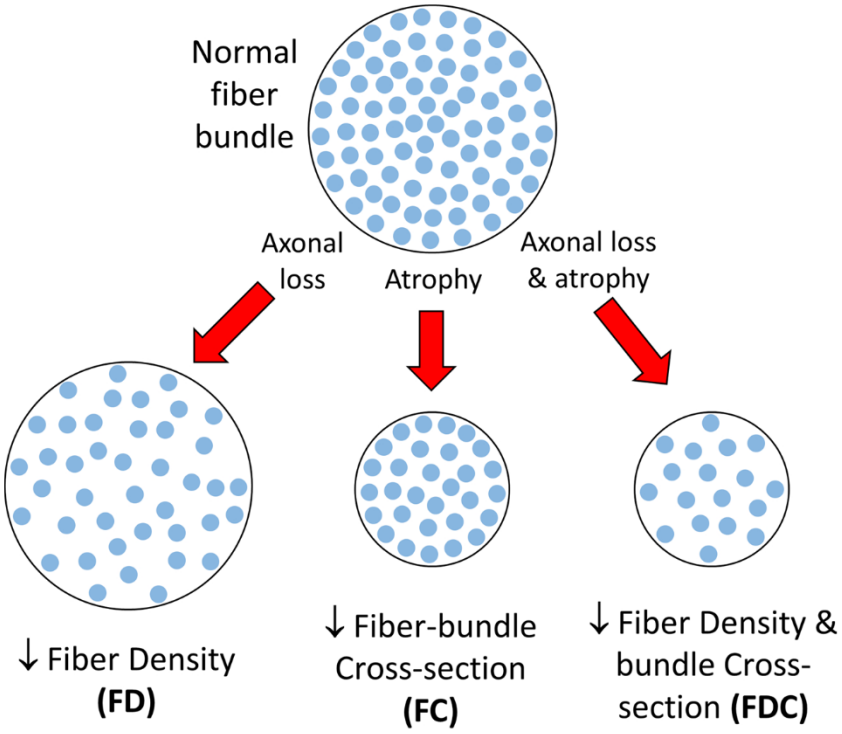

Fig. 1. Schematic of fiber bundle cross-sections exhibiting changes in FBA measures. Blue circles represent cross-sections of axons within a fiber bundle. A decrease in FD represents a loss of axonal density. A decrease in FC represents morphological atrophy of a fiber bundle. A decrease of FDC represents both a loss of axonal density and atrophy of a fiber bundle (Figure adapted from Raffelt et al. [16]).

were included in this study.

2.3. Ophthalmic tests

All participants underwent visual acuity, tonometry, optical coherence tomography (OCT) and standard automated perimetry exams. Visual acuity was tested using Snellen charts with optimal correction for the viewing distance. Tonometry was performed using a Tonoref non-contact tonometer (Nidek, Hiroishi, Japan). A Canon OCT-HS100 scanner (Canon, Tokyo, Japan) was used to measure the average peripapillary RNFL (pRNFL) thickness. For glaucoma patients, perimetry was performed using a Humphrey Field Analyzer (HFA; Carl Zeiss

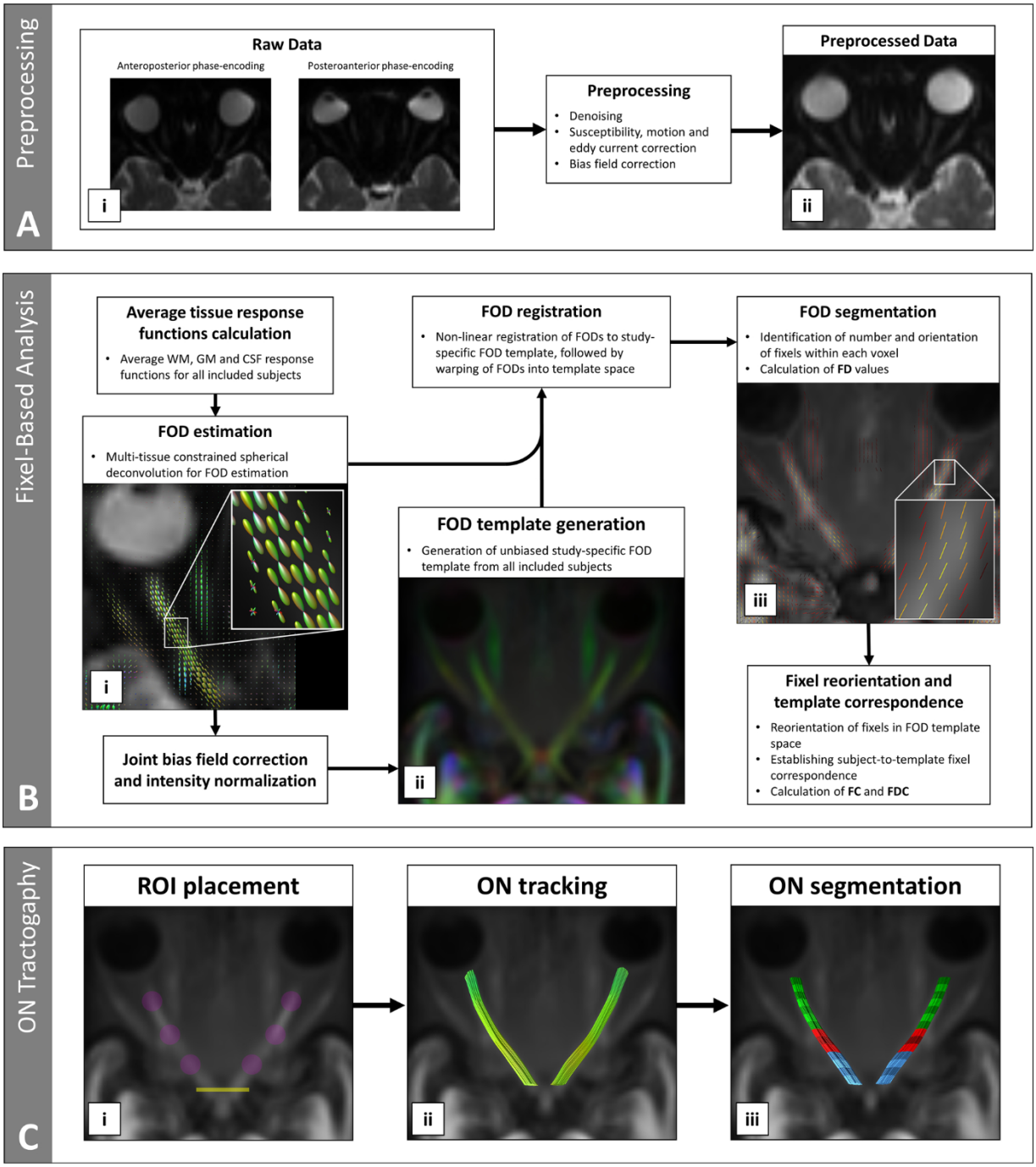

Fig. 2. Overview of data analysis pipeline. (A) Preprocessing of raw DWI data. i) Example of single subject DWI scans acquired using anteroposterior and posteroanterior phase-encoding directions, ii) Preprocessed DWI scan of the same subject; (B) Fixel-based analysis. i) A close-up view of FODs estimated for a single subject. Zoomed inset shows FODs in a segment of the optic nerve (ON), ii) Cropped image of the produced population template, color-coded based on the directionality of diffusion, iii) Cropped image of identified fixels in a single subject. Fixels are color-coded based on their fiber density (FD) values, with yellow representing higher FD and red representing lower FD. Zoomed inset shows fixels in a segment of the ON; C) ON tracking and segmentation. i) Placement of regions of interest (ROIs). Yellow: optic chiasm ROI; magenta: visual representation of spherical ROIs placed along the ONs. ii) The result of deterministic tracking between the ROIs, color-coded by directionality. iii) ON segmentation. Each optic nerve is segmented into 14 sub-segments, and each sub-segment is assigned to an anatomical ON segment. Alternating shades of the same color represent different sub-segments of the same anatomical segment. Green: intraorbital segment; red: intracanalicular segment; blue: intracranial segment.

Meditec, Jena, Germany) using the 30−2 grid and the Swedish Interactive Threshold Algorithm (SITA), and the results were expressed as visual field mean deviation (VFMD). For controls, perimetry was performed using Frequency Doubling Technology (FDT; Carl Zeiss Meditec, Jena, Germany) with the C20−1 screening mode to exclude controls with any visual field defects.

2.4. DWI data acquisition

Whole-brain DWI scans were acquired on a Siemens MAGNETOM Prisma 3 T MRI scanner (Siemens, Erlangen, Germany) with a 64-channel head coil. The following parameters were used for data acquisition: echo-time/repetition time (TE/TR) = 85/5500 ms, 66 axial slices, slice thickness = 2 mm, voxel size = 2 mm isotropic, field of view (FoV) = 210 × 210 mm, 2 DWI shells (b = 1000s/mm^2 and b = 2500s/mm^2), 64 diffusion gradient directions for each shell in two phase-encoding directions (anteroposterior and posteroanterior), and 3 non-diffusion weighted images (b = 0 s/mm^2) in each phase-encoding direction (6 in total). During scanning, we ensured the inclusion of the entire length and thickness of both ONs in the FoV of each participant. The participants were asked to close their eyelids and reduce eye movements during the scan as much as possible.

2.5. Data preprocessing

The images were first denoised [18], then corrected for susceptibility [19], motion, and eddy current induced distortions [20] using FMRIB's Software Library (FSL v5.011, https://fsl.fmrib.ox.ac.uk/fsl), and finally corrected for bias field inhomogeneity [21]. The images were then visually inspected for any uncorrected motion artifacts of the ONs.

2.6. Fixel-based analysis

The complete FBA pipeline has been previously described in detail by Raffelt et al. [16]. Here, we briefly give an overview of the main steps of FBA, and specifically highlight any performed analyses which deviate from the default FBA pipeline. All described steps have been performed in MRtrix3 (www.mrtrix.org) [22]. A summary of the main steps of this study's pipeline is illustrated in Fig. 2.

First, average tissue response functions were produced from the WM, grey matter, and cerebrospinal fluid of all included subjects [23]. Then, all images were upsampled to an isotropic voxel size of 1.3 mm. Next, brain masks were computed for the upsampled images and manually edited to include the ONs. Multi-tissue constrained spherical deconvolution [24] was then performed using the produced set of average tissue response functions to estimate fiber orientation distributions (FODs) for each subject, followed by joint bias field correction and intensity normalization [17].

A group-specific FOD template was produced from all 30 included subjects [25], and all FODs were then non-linearly registered to the FOD template space to attain spatial correspondence [26]. Subsequently, the FOD lobes were segmented to identify the number and orientation of fixels within each voxel, and the fixels were assigned FD values based on the amplitude of the FOD lobes. Then, the fixels were reoriented in FOD template space based on the non-linear transformation of their corresponding voxels, and then assigned to their spatially corresponding template fixels. The FC was then computed for each fixel based on the warps produced during registration. Finally, the FDC was calculated based on the computed FD and FC values.

2.7. Optic nerve tracking and segmentation

In order to analyze the ONs, deterministic tractography was used to track the ONs in the FOD template space (Fig. 2C). The tracking was performed using 3 spherical inclusion regions of interest (ROIs) placed along the length of both ONs and a single rectangular inclusion ROI at the optic chiasm. All 3 ON inclusion ROIs measured 2 mm in radius, and were placed manually in the center of the ON at approximately the middle of the IO segment, the distal opening of the optic canal and the middle of the ICRAN segment. The optic chiasm ROI was created in the coronal plane, measuring 7 × 15 × 1 voxels (9.1 × 19.5 × 1.3 mm).

Following ON tracking, approximately 3 mm of the distal ends of the ONs were excluded from the analysis to avoid signal contamination from the posterior poles of the eye globes [12,27]. The ONs were then segmented into 14 sub-segments of equal coronal thickness, each segment measuring 2.6 mm (or the equivalent of 2 slices) in thickness. The resulting ON sub-segments were then numbered in ascending order, starting at the sub-segments closest to the eye globes and ending at the optic chiasm. Then, each sub-segment was assigned to one of the three anatomical segments of the ON; intraorbital (IO), intracanalicular (ICAN) or intracranial (ICRAN) segment. The categorization was done based on visual inspection of anatomical landmarks and the surroundings of the ON. The IO was identified as the segment starting at the posterior pole of the eye globe and ending at the apex of the orbit, marked by the origin of the extraocular rectus muscles (annulus of Zinn). Seven sub-segments (1–7) were assigned to the IO segment. The ICRAN was identified as the segment emerging from the proximal end of the optic canal to enter the cranial cavity and ending at the optic chiasm. Four sub-segments (11–14) were assigned to the ICRAN. The ICAN was determined as the segment between the IO and ICRAN (sub-segments 8–10).

Finally, the FD, FC and FDC values were computed for each of the 14 sub-segments. The FD was computed using the Apparent Fiber Density framework described by Raffelt et al. [17], where the amplitude of an FOD along a WM fiber population is assumed to represent the within-voxel volume occupied by the axons of that specific fiber population. The FC was calculated using the non-linear warps required to co-register the fixels of each subject to the population template, where a positive FC indicates a cross-sectional area greater than that of the population template and a negative FC represents a cross-sectional area smaller than that of the population template. The FDC was computed as described by Raffelt et al. [16], to incorporate both FD and FC, providing a measure which takes into account both micro- and macrostructural changes.

2.8. DTI analysis

For comparison, a conventional voxel-based DTI analysis was also performed. First, diffusion tensors were produced from the b = 0 s/mm^2 and b = 1000s/mm^2 shells of the preprocessed diffusion data. Then, FA and MD maps were derived from the tensors. The maps were then warped to the FOD template space using the same non-linear subject-to-template warps produced during FOD registration. Voxel-based masks for each of the 14 ON sub-segments were also created. Finally, the FA and MD of each sub-segment were computed.

2.9. Statistical analysis

As some of the glaucoma patients were affected unilaterally and others bilaterally, a single ON was included from each patient for statistical analysis. For unilaterally affected patients, the glaucomatous ON was included; for bilaterally affected patients, a single ON was randomly selected. For the control group, a single random ON was included for each subject, ensuring to keep the same right-to-left side ratio as the glaucoma group. In total, 9 right-sided and 6 left-sided ONs were included from both groups.

To analyze the patients' demographics and clinical characteristics of the included ONs, independent-samples *t*-test was used for parametric continuous variables, Mann-Whitney *U* test was used for non-parametric continuous variables, and χ^2 test was used for categorical variables. Statistical significance was reported at $P < 0.05$.

To compare FBA and DTI measures of each ON sub-segment between

the two groups, analysis of covariance (ANCOVA) was used, while controlling for age and sex as nuisance co-variates. To study the three ON anatomical segments, FBA measures were first averaged for each segment, then ANCOVA was also used to compare the measures of each anatomical segment between the two groups. False discovery rate (FDR) was used to correct for multiple comparisons, and statistical significance was reported at $P_{FDR} < 0.05$. A within-subject comparison between the average FBA measures of each ON segment was performed for the controls and glaucoma patients using within-subjects ANOVA, and statistical significance was reported at a post-hoc Bonferroni corrected $P < 0.05$. Spearman's rank correlation analysis was used to study the correlation between the average FBA and DTI measures of each anatomical segment of the glaucomatous ONs and the average pRNFL thickness and VFMD. A Spearman's correlation coefficient (ρ) ≤ 0.3 signified a very weak correlation, $0.3 < \rho \leq 0.5$ signified a weak correlation, $0.5 < \rho \leq 0.7$ signified a moderate correlation, and $\rho > 0.7$ signified a strong correlation. Statistical significance was reported at $P < 0.05$.

3. Results

3.1. Demographics and clinical characteristics

A summary of participants' demographics and the clinical characteristics of the eyes corresponding to the included ONs can be found in Table 1. The two groups did not differ significantly in age, sex or IOP. Visual acuity and pRNFL thickness were significantly lower in the glaucoma group. The glaucoma group included twelve primary open-angle glaucoma (POAG) patients, two pseudoexfoliative glaucoma (PEX) patients and a single case of pigmentary glaucoma (PG). Based on the Hodapp-Parrish-Anderson (H-P-A) classification, the included eyes comprised four early stage, two moderate, five advanced, and four severe glaucomatous eyes.

3.2. Fixel-wise analysis

All sub-segments of the glaucomatous ONs showed a significant decrease ($P_{FDR} < 0.05$) in FD and FDC compared to the controls, while only sub-segments 2–5 and 12–14 showed a significant loss of FC (Fig. 3). Group difference effect sizes for different FBA measures along the ONs are illustrated in Fig. 4. A detailed list of the FBA measures of each sub-segment and their corresponding group difference p-values and effect sizes can be found in Supplementary Table 1. The average of each anatomical ON segment showed a significant decrease in FD and FDC in all three segments ($P_{FDR} < 0.05$), and a significant decrease of FC in the IO and ICRAN segments only (Table 2).

Table 1
Group demographics and clinical characteristics of included ONs.

	Glaucoma (n = 15)	Controls (n = 15)	*P*
Age (years)	67.6(7.4)	70.1(7.4)	0.44
Males (%)	8(53.3 %)	8(53.3 %)	1.00
Visual acuity	0.88(0.25)	1.14(0.30)	0.02
IOP recorded during study (mmHg)	13.5(4.3)	12.1(3.8)	0.48
pRNFL (μm)	65.1(7.4)	99.5(7.8)	<0.001
VFMD (dB)	−14.9(9.9)	–	–
Glaucoma subtype			
POAG	12(80 %)	–	–
PEX	2(13.3 %)	–	–
PG	1(6.7 %)	–	–
H-P-A stage			
1	4(26.7 %)	–	–
2	2(13.3 %)	–	–
3	5(33.3 %)	–	–
4	4(26.7 %)	–	–

Values are presented as mean (SD) or number (%). IOP = intraocular pressure; H-P-A = Hodapp-Parrish-Anderson classification; PEX = pseudoexfoliative glaucoma; PG = pigmentary glaucoma; POAG = primary open-angle glaucoma; pRNFL = peripapillary retinal nerve fiber layer; VFMD = visual field mean deviation.

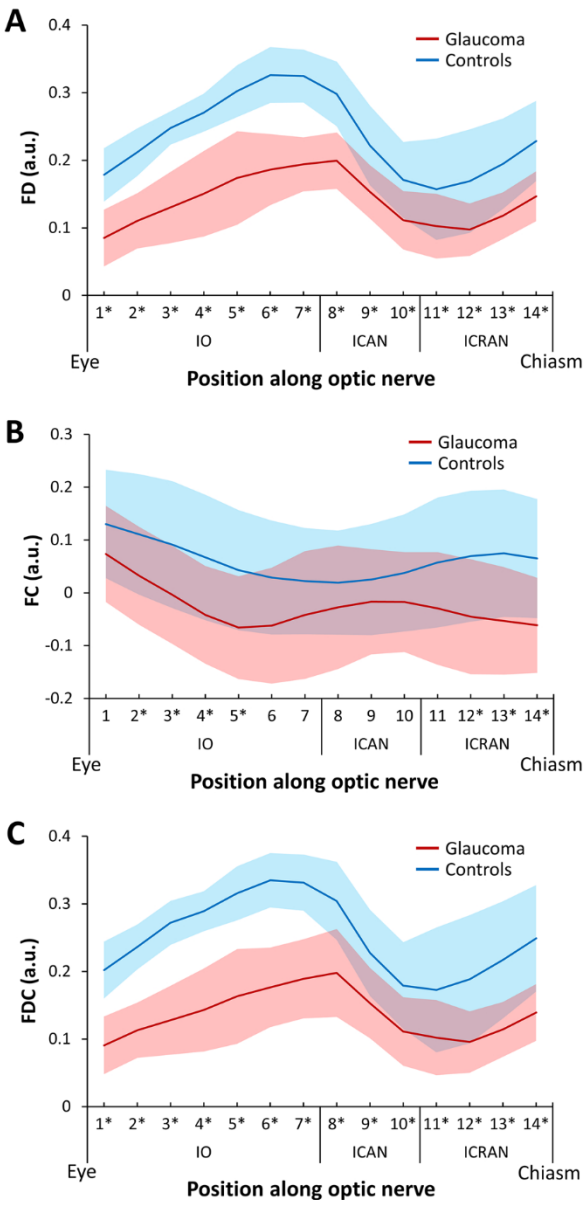

Fig. 3. Fixel-based analysis measures along the optic nerves of the glaucoma and control groups. FD (**A**), FC (**B**) and FDC (**C**) measures along the length of glaucomatous and control optic nerves. Solid lines represent group mean; transparent ribbons represent SD; * indicates sub-segments showing statistically significant difference between the groups ($P_{FDR} < 0.05$). FC = fiber-bundle cross-section; FD = fiber density; FDC = fiber density and cross-section; ICAN = intracanalicular; ICRAN = intracranial; IO = intraorbital.

3.3. DTI analysis

Sub-segments 2–14 of the glaucomatous ONs showed a significant decrease ($P_{FDR} < 0.05$) in FA compared to the controls, while only sub-segment 14 showed a significant increase of MD (Fig. 5). Group difference effect sizes for FA and MD along the ONs are illustrated alongside their FBA counterparts for comparison in Fig. 4. A detailed list of the DTI measures of each sub-segment and their corresponding group difference p-values and effect sizes can be found in Supplementary Table 2. The average of each anatomical ON segment showed a significant decrease in FA in all three segments ($P_{FDR} < 0.05$), and a significant increase of MD

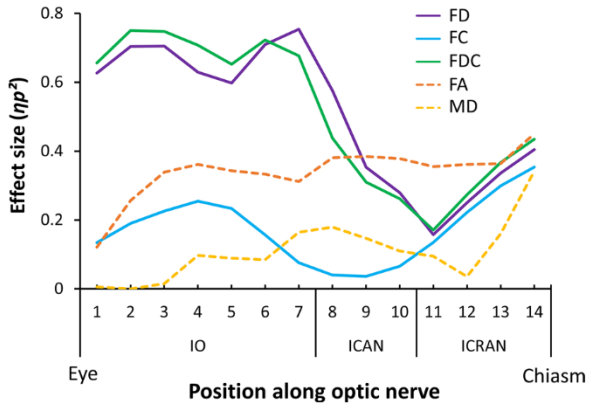

Fig. 4. Group difference effects sizes for fixel- and tensor-based measures. Effect sizes of group differences between glaucoma and control groups along the length of their optic nerves for both fixel-based (FD, FC, and FDC; solid lines) and tensor-based (FA and MD; dashed lines) measures. All effect size values are plotted regardless of statistical significance. FA = fractional anisotropy; FC = fiber-bundle cross-section; FD = fiber density; FDC = fiber density and cross-section; ICAN = intracanalicular; ICRAN = intracranial; IO = intraorbital; MD = mean diffusivity.

Table 2
Comparison of FBA and DTI measures of ON segments between glaucoma patients and controls.

	Anatomical segment	Glaucoma (n = 15)	Controls (n = 15)	Effect size (ηp^2)	P_{FDR}
FBA measure					
FD	IO	0.15(0.05)	0.27(0.03)	0.72	**<0.001**
	ICAN	0.15(0.03)	0.23(0.05)	0.49	**<0.001**
	ICRAN	0.12(0.03)	0.19(0.06)	0.33	**<0.01**
FC	IO	−0.02(0.09)	0.07(0.11)	0.20	**0.03**
	ICAN	−0.02(0.10)	0.03(0.10)	0.05	0.24
	ICRAN	−0.05(0.10)	0.07(0.12)	0.26	**0.02**
FDC	IO	0.14(0.05)	0.28(0.03)	0.75	**<0.001**
	ICAN	0.15(0.05)	0.24(0.05)	0.42	**<0.001**
	ICRAN	0.11(0.04)	0.21(0.08)	0.35	**<0.001**
DTI measure					
FA	IO	0.21(0.08)	0.32(0.07)	0.36	**<0.001**
	ICAN	0.27(0.07)	0.39(0.06)	0.47	**<0.001**
	ICRAN	0.18(0.03)	0.25(0.04)	0.53	**<0.001**
MD	IO	1.48(0.32)	1.37(0.24)	0.04	0.33
	ICAN	1.05(0.25)	0.86(0.15)	0.19	0.06
	ICRAN	1.42(0.30)	1.21(0.31)	0.19	**0.03**

Values are presented as mean (SD). FA = fractional anisotropy; FC = fiber-bundle cross-section; FD = fiber density; FDC = fiber density and cross-section; ICAN = intracanalicular; ICRAN = intracranial; IO = intraorbital; MD = mean diffusivity.

in the ICRAN segment only (Table 2).

3.4. Within-subject comparison of ON segments

For the glaucoma group, FD was significantly higher in the IO and ICAN segments compared to the ICRAN segment ($P = 0.044$ and $P = 0.001$, respectively) and FDC was higher in the ICAN segment compared to the ICRAN segment ($P = 0.010$). For the control group, FD was significantly higher in the IO segment compared to the ICAN and ICRAN segments ($P = 0.023$ and $P = 0.001$, respectively) and FDC was higher in the IO segment compared to the ICAN and ICRAN segments ($P = 0.016$ and $P = 0.006$, respectively). FC showed no difference between segments in both groups.

3.5. Correlation with ophthalmic tests

Average FBA and DTI measures of the anatomical segments of

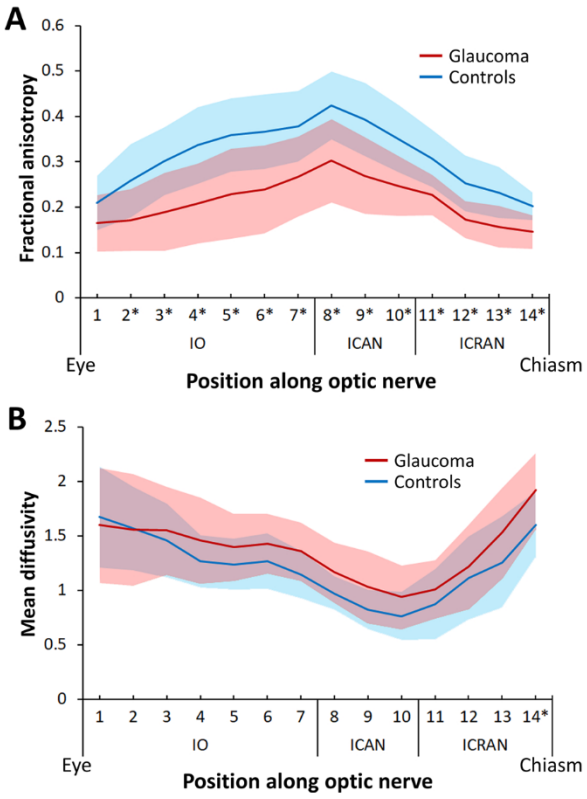

Fig. 5. Tensor-based measures along the optic nerves of the glaucoma and control groups. FA (**A**) and MD (**B**) measures along length of glaucomatous and control optic nerves. Solid lines represent group mean; transparent ribbons represent SD; * indicates sub-segments showing statistically significant difference between the groups ($P_{FDR} < 0.05$). FA = fractional anisotropy; ICAN = intracanalicular; ICRAN = intracranial; IO = intraorbital; MD = mean diffusivity.

glaucomatous ONs showed varying degrees of correlation with the average pRNFL thickness and the VFMD (Table 3). The strongest correlation was found between the FDC of the IO segment and VFMD ($\rho^2 = 0.83$, $P < 0.001$), while the FC of all segments showed no correlation

Table 3
Correlation between FBA and DTI measures of glaucomatous ON segments and ophthalmic tests.

	Anatomical segment	Average pRNFL		VFMD	
		ρ^2	P	ρ^2	P
FBA measure					
FD	IO	0.47	**<0.01**	0.76	**<0.001**
	ICAN	0.53	**<0.01**	0.53	**<0.01**
	ICRAN	0.34	**0.02**	0.26	0.05
FC	IO	0.01	0.77	0.00	0.85
	ICAN	0.02	0.58	0.14	0.16
	ICRAN	0.08	0.3	0.07	0.33
FDC	IO	0.52	**<0.01**	0.83	**<0.001**
	ICAN	0.28	**0.04**	0.39	**0.01**
	ICRAN	0.30	**0.03**	0.21	0.09
DTI measure					
FA	IO	0.25	0.06	0.37	**0.02**
	ICAN	0.34	**0.02**	0.56	**<0.01**
	ICRAN	0.08	0.30	0.07	0.35
MD	IO	−0.02	0.61	−0.15	0.16
	ICAN	−0.19	0.10	−0.47	**<0.01**
	ICRAN	0.11	0.23	0.07	0.35

FA = fractional anisotropy; FC = fiber-bundle cross-section; FD = fiber density; FDC = fiber density and cross-section; ICAN = intracanalicular; ICRAN = intracranial; IO = intraorbital; MD = mean diffusivity; pRNFL = peripapillary retinal nerve fiber layer; VFMD = visual field mean deviation.

with either of the ophthalmic tests.

4. Discussion

This study presents the first application of FBA to characterize glaucomatous ON degeneration. We find that glaucomatous ONs show axonal loss and decreased cross-sectional area compared to healthy subjects. Furthermore, we find a strong correlation between FBA measures and both functional and structural glaucoma tests. This suggests the viability of FBA measures as potential biomarkers of glaucomatous ON degeneration.

4.1. Glaucomatous ONs exhibit axonal loss

Glaucomatous ONs showed a decrease of FD along their entire length, indicating axonal loss. This finding is in line with our knowledge of glaucoma as a degenerative disease of the RGCs and their ON-forming axons. This axonal loss has been previously reported by Gupta et al. in the only human postmortem study of the ONs of a glaucoma patient [28]. Specifically, axonal loss was found to be more evident inferiorly in both ONs, which corresponded with a bilateral superior visual field loss experienced by the patient [28]. Although Gupta et al. analyzed only the ICRAN segments of the ONs, there is no reason to believe the other ON segments would have shown different results. Furthermore, studies of primate glaucoma models found a similar loss of axons in the IO segments of the ONs following the induction of experimental glaucoma [29,30].

While all anatomical segments of the glaucomatous ONs showed a significant decrease in FD, the effect size of this decrease appears to be considerably higher at the IO segment. From a histopathological perspective, we expect axonal loss to be uniform throughout the length of the ON. Therefore, this variation in effect size along the ON is most likely due to technical limitations of DWI. The skull base and air-filled paranasal sinuses adjacent to the ONs create susceptibility-induced magnetic field inhomogeneities, which can cause geometric distortions and signal loss [27,31]. These magnetic susceptibility artifacts are more likely to affect the ICAN and ICRAN segments, as they are in closer proximity to the magnetic field distortions compared to the IO segment, which explains the lower effect sizes found in these segments. This, in addition to the within-subject FD differences we found between the ON segments, highlights the importance of assessing the entire length of the ON to overcome some the limitations of DWI of the ON and to gain a more complete picture of glaucomatous ON degeneration.

4.2. Segment-specific atrophy of glaucomatous ONs

Glaucomatous ONs showed atrophic changes (as indicated by a decrease in FC) at the IO and ICRAN segments, but not the ICAN segment. The aforementioned postmortem and primate studies have also found macrostructural atrophy in the ICRAN and IO segments, respectively [28,30]. Moreover, structural MRI studies of glaucomatous ONs have also reported a decrease in diamet er [4,32–34] and cross-sectional area [35,36] of the IO segment. However, no previous study has specifically reported on morphological changes in the ICAN segment of glaucomatous ONs, most likely due to its inconvenient position within the bony optic canal.

The cause of this lack of atrophy at the ICAN segments of glaucomatous ONs in the present study is unclear. However, it is most likely a true reflection of ON morphology and not a result of imaging limitations. This is evident from the different patterns of FC changes along the glaucomatous and healthy ONs, where the FC values converge at the ICAN compared to other segments, producing a bottleneck-like effect (Fig. 3B). This finding further demonstrates the importance of assessing the entire length of glaucomatous ONs.

4.3. DTI analysis in comparison to FBA

All three anatomical segments of the glaucomatous ONs showed a decrease in FA, which lacks an explicit biological interpretation and rather indicates a general loss of structural integrity. This is in agreement with other DTI studies of glaucomatous ONs [3–12], the majority of which investigated the IO segment only. While the loss of FA in the IO segment in our study was significant, it had a considerably lower effect size compared to the FD and FDC values of the same segment. This can be explained by the aforementioned limitations of the tensor-model, especially partial volume effects produced by the cerebrospinal fluid surrounding the ON. Interestingly, the effect size of FA loss showed a relatively flat profile along the ON, and did not exhibit the same noticeable decline found with FD at the ICAN and ICRAN segments (Fig. 4). This could be due to the fact that our DTI analysis utilized only the low b-value shell for tensor fitting, while FBA used the high b-value shell as well, which is associated with lower signal-to-noise ratio and greater geometric distortions [37], to which the ICAN and ICRAN segments are susceptible due to their anatomical proximity to the skull base and paranasal sinuses.

4.4. FBA measures as biomarkers of glaucomatous ON degeneration

A moderate to strong correlation was found between the FD of the glaucomatous ONs and the average pRNFL thickness and VFMD. This correlation is expected, as a decrease in FD represents a loss of RGC axons, which reflects a loss of structure and function of the RGCs at the level of the retina. A primate study found a similar correlation between the RNFL thickness and nerve fiber density in ONs with experimentally induced glaucoma [29]. FC of the glaucomatous ONs, however, showed no significant correlation with either of the ophthalmic tests. This is most likely due to the difference in scale between these tests, as the FC is a coarse measurement of gross morphological changes while the ophthalmic tests operate on a much finer scale. The FDC showed the strongest correlation with the ophthalmic tests, specifically at the IO segment. As FDC is a combination of both FD and FC, it is supposed to represent the overall information carrying capacity of the ONs, which explains its strong correlation with the ophthalmic tests. This finding suggests that FDC of the IO segment offers the most accurate representation of glaucomatous ON degeneration and hence shows the most potential for being used as a biomarker of glaucomatous ON degeneration.

4.5. Comparison to previous FBA studies

In a previous study, we utilized FBA to investigate post-chiasmatic visual pathway changes in POAG patients to better understand the underlying pathophysiology of the central degeneration found in these patients [38]. We found a significant loss of FD, FC and FDC in the optic tracts (OTs) of POAG patients, which is in line with our current findings as the OTs and ONs are both formed of RGC axons. However, as the OTs are partially formed of RGC axons which cross the midline at the chiasm, they cannot be directly probed to assess glaucomatous degeneration affecting a single eye. In our current study, we focused on characterizing degenerative changes along glaucomatous ONs using FBA and evaluating the potential of FBA measures along the ONs as direct biomarkers for glaucomatous degeneration.

4.6. Clinical implications

Currently, OCT is the most widely used ophthalmic test for assessing structural degeneration in glaucoma. However, OCT has a number of limitations. For example, OCT measurements of RNFL thickness exhibit a so-called “floor effect”, where visual field loss continues progressing while detectable thinning of the RNFL plateaus [39]. This limits the ability of OCT to follow disease progression in advanced glaucoma.

Furthermore, the presence of ocular media opacities (for example, a dense cataract or corneal scarring) can influence the reliability of OCT measurements [40]. Given the irreversible nature of glaucomatous damage, a diagnostic test circumventing the limitations of OCT could improve glaucoma patient care. FBA measures show promise as potential biomarkers of structural glaucomatous degeneration, and hence could prove to be a viable alternative, or at the very least a complementary test, to OCT in the future. In addition to its potential for clinical use, FBA could also be of value to the in vivo testing of novel glaucoma therapies such as RGC transplantation [41] and neuroprotection [42].

4.7. Study limitations and future directions

The present study has a number of limitations. Firstly, the number of participants is moderate. However, our group sizes are still in line with previous DWI studies of glaucoma [3,12,43–46]. Future studies could benefit from a larger sample size and a separate analysis of different stages of glaucoma. Furthermore, a normative database including representative samples of normal ONs of different age groups, genders and ethnicities would be needed to make FBA measures of ONs clinically applicable.

Another limitation is the relatively low resolution of the DWI scans in comparison to ON size. However, this limitation is not specific to our study, but is rather a general limitation of imaging small structures like the ON using DWI. Optimizing a DWI protocol for ON imaging and using a dedicated surface coil could increase image resolution and reduce scanning time considerably, making FBA a more feasible clinical tool for assessing ON structural changes in glaucoma.

5. Conclusions

Using FBA, we were able to detect axonal loss (as indicated by FD loss) and gross atrophy (as indicated by FC decrease) along the different anatomical segments of glaucomatous ONs. Our findings are congruent with postmortem and primate studies of glaucomatous ON pathology. Compared to conventional voxel-based DTI, FBA provides more biologically meaningful measures of glaucomatous ON degeneration. Furthermore, FBA measures of glaucomatous ON degeneration show a strong correlation with the outcomes of established ophthalmic tests of glaucoma. This suggests a potential for FBA measures to serve as biomarkers of glaucomatous ON degeneration, in particular in conditions where current ophthalmic imaging techniques are unable to trace such degeneration.

Funding

This work was supported by the European Union's Horizon 2020 research and innovation programme under the Marie Sklodowska-Curie grant agreement No. 675033 (Egret-plus). SH was also supported by The Graduate School of Medical Sciences (GSMS), University of Groningen, The Netherlands. The funding organizations had no role in the design, conduct, analysis, or publication of this research.

CRediT authorship contribution statement

Shereif Haykal: Conceptualization, Methodology, Investigation, Data curation, Writing - original draft, Visualization. **Nomdo M. Jansonius:** Conceptualization, Resources, Writing - review & editing, Supervision, Funding acquisition. **Frans W. Cornelissen:** Conceptualization, Resources, Writing - review & editing, Visualization, Supervision, Funding acquisition.

Declaration of Competing Interest

None.

Appendix A. Supplementary data

Supplementary material related to this article can be found, in the online version, at doi:https://doi.org/10.1016/j.ejrad.2020.109356.

References

[1] R.J. Casson, G. Chidlow, J.P.M. Wood, J.G. Crowston, I. Goldberg, Definition of glaucoma: clinical and experimental concepts, Clin. Experiment. Ophthalmol. 40 (2012) 341–349, https://doi.org/10.1111/j.1442-9071.2012.02773.x.
[2] D.J. Calkins, P.J. Horner, The cell and molecular biology of glaucoma: axonopathy and the brain, Invest. Ophthalmol. Vis. Sci. 53 (2012) 2482–2484, https://doi.org/10.1167/iovs.12-9483i.
[3] F.G. Garaci, F. Bolacchi, A. Cerulli, M. Melis, A. Spanò, C. Cedrone, R. Floris, G. Simonetti, C. Nucci, Optic nerve and optic radiation neurodegeneration in patients with glaucoma: in vivo analysis with 3-T diffusion-tensor MR imaging, Radiology. 252 (2009) 496–501, https://doi.org/10.1148/radiol.2522081240.
[4] Y.Q. Zhang, J. Li, L. Xu, L. Zhang, Z.C. Wang, H. Yang, C.X. Chen, X.S. Wu, J. B. Jonas, Anterior visual pathway assessment by magnetic resonance imaging in normal-pressure glaucoma, Acta Ophthalmol. 90 (2012) e295–302, https://doi.org/10.1111/j.1755-3768.2011.02346.x.
[5] F. Bolacchi, F.G. Garaci, A. Martucci, A. Meschini, M. Fornari, S. Marziali, R. Mancino, E. Squillaci, R. Floris, L. Cerulli, G. Simonetti, C. Nucci, Differences between proximal versus distal intraorbital optic nerve diffusion tensor magnetic resonance imaging properties in glaucoma patients, Invest. Ophthalmol. Vis. Sci. 53 (2012) 4191–4196, https://doi.org/10.1167/iovs.11-9345.
[6] C. Nucci, R. Mancino, A. Martucci, F. Bolacchi, G. Manenti, C. Cedrone, F. Culasso, R. Floris, L. Cerulli, F.G. Garaci, 3-T Diffusion tensor imaging of the optic nerve in subjects with glaucoma: correlation with GDx-VCC, HRT-III and Stratus optical coherence tomography findings, Br. J. Ophthalmol. 96 (2012) 976–980, https://doi.org/10.1136/bjophthalmol-2011-301280.
[7] M.-Y. Wang, K. Wu, J.-M. Xu, J. Dai, W. Qin, J. Liu, J. Tian, D. Shi, Quantitative 3-T diffusion tensor imaging in detecting optic nerve degeneration in patients with glaucoma: association with retinal nerve fiber layer thickness and clinical severity, Neuroradiology. 55 (2013) 493–498, https://doi.org/10.1007/s00234-013-1133-1.
[8] S.T. Chang, J. Xu, K. Trinkaus, M. Pekmezci, S.N. Arthur, S.-K. Song, E.M. Barnett, Optic nerve diffusion tensor imaging parameters and their correlation with optic disc topography and disease severity in adult glaucoma patients and controls, J. Glaucoma 23 (2013) 513–520, https://doi.org/10.1097/IJG.0b013e318294861d.
[9] K. Omodaka, T. Murata, S. Sato, M. Takahashi, Y. Tatewaki, T. Nagasaka, H. Doi, M. Araie, S. Takahashi, T. Nakazawa, Correlation of magnetic resonance imaging optic nerve parameters to optical coherence tomography and the visual field in glaucoma, Clin. Experiment. Ophthalmol. 42 (2014) 360–368, https://doi.org/10.1111/ceo.12237.
[10] S. Sidek, N. Ramli, K. Rahmat, N.M. Ramli, F. Abdulrahman, L.K. Tan, Glaucoma severity affects diffusion tensor imaging (DTI) parameters of the optic nerve and optic radiation, Eur. J. Radiol. 83 (2014) 1437–1441, https://doi.org/10.1016/j.ejrad.2014.05.014.
[11] Q.-J. Zhang, D. Wang, Z.-L. Bai, B.-C. Ren, X.-H. Li, Diffusion tensor imaging of optic nerve and optic radiation in primary chronic angle-closure glaucoma using 3T magnetic resonance imaging, Int. J. Ophthalmol. 8 (2015) 975–979, https://doi.org/10.3980/j.issn.2222-3959.2015.05.22.
[12] N. Miller, Y. Liu, R. Krivochenitser, B. Rokers, Linking neural and clinical measures of glaucoma with diffusion magnetic resonance imaging (dMRI), PLoS One 14 (2019), e0217011, https://doi.org/10.1371/journal.pone.0217011.
[13] L.J. O'Donnell, C.-F. Westin, An introduction to diffusion tensor image analysis, Neurosurg. Clin. N. Am. 22 (2011) 185–196, https://doi.org/10.1016/j.nec.2010.12.004, viii.
[14] D.K. Jones, T.R. Knösche, R. Turner, White matter integrity, fiber count, and other fallacies: the do's and don'ts of diffusion MRI, Neuroimage. 73 (2013) 239–254, https://doi.org/10.1016/j.neuroimage.2012.06.081.
[15] A.L. Alexander, K.M. Hasan, M. Lazar, J.S. Tsuruda, D.L. Parker, Analysis of partial volume effects in diffusion-tensor MRI, Magn. Reson. Med. 45 (2001) 770–780, https://doi.org/10.1002/mrm.1105.
[16] D.A. Raffelt, J.-D. Tournier, R.E. Smith, D.N. Vaughan, G. Jackson, G.R. Ridgway, A. Connelly, Investigating white matter fibre density and morphology using fixel-based analysis, Neuroimage. 144 (2017) 58–73, https://doi.org/10.1016/j.neuroimage.2016.09.029.
[17] D. Raffelt, J.-D. Tournier, S. Rose, G.R. Ridgway, R. Henderson, S. Crozier, O. Salvado, A. Connelly, Apparent Fibre Density: a novel measure for the analysis of diffusion-weighted magnetic resonance images, Neuroimage. 59 (2012) 3976–3994, https://doi.org/10.1016/j.neuroimage.2011.10.045.
[18] J. Veraart, E. Fieremans, D.S. Novikov, Diffusion MRI noise mapping using random matrix theory, Magn. Reson. Med. 76 (2016) 1582–1593, https://doi.org/10.1002/mrm.26059.
[19] J.L.R. Andersson, S. Skare, J. Ashburner, How to correct susceptibility distortions in spin-echo echo-planar images: application to diffusion tensor imaging, Neuroimage. 20 (2003) 870–888, https://doi.org/10.1016/S1053-8119(03)00336-7.
[20] J.L.R. Andersson, S.N. Sotiropoulos, An integrated approach to correction for off-resonance effects and subject movement in diffusion MR imaging, Neuroimage. 125 (2016) 1063–1078, https://doi.org/10.1016/j.neuroimage.2015.10.019.

[21] N.J. Tustison, B.B. Avants, P.A. Cook, Y. Zheng, A. Egan, P.A. Yushkevich, J.C. Gee, N4ITK: improved N3 bias correction, IEEE Trans. Med. Imaging 29 (2010) 1310–1320, https://doi.org/10.1109/TMI.2010.2046908.
[22] J.-D. Tournier, R. Smith, D. Raffelt, R. Tabbara, T. Dhollander, M. Pietsch, D. Christiaens, B. Jeurissen, C.-H. Yeh, A. Connelly, MRtrix3: A fast, flexible and open software framework for medical image processing and visualisation, Neuroimage. 202 (2019), 116137, https://doi.org/10.1016/j.neuroimage.2019.116137.
[23] T. Dhollander, D. Raffelt, A. Connelly, Unsupervised 3-tissue response function estimation from single-shell or multi-shell diffusion MR data without a co-registered T1 image, ISMRM Work. Break. Barriers Diffus. MRI (2016) 5. https://www.researchgate.net/publication/307863133_Unsupervised_3-tissue_response_function_estimation_from_single-shell_or_multi-shell_diffusion_MR_data_without_a_co-registered_T1_image.
[24] B. Jeurissen, J.-D. Tournier, T. Dhollander, A. Connelly, J. Sijbers, Multi-tissue constrained spherical deconvolution for improved analysis of multi-shell diffusion MRI data, Neuroimage. 103 (2014) 411–426, https://doi.org/10.1016/j.neuroimage.2014.07.061.
[25] D. Raffelt, J.-D. Tournier, J. Fripp, S. Crozier, A. Connelly, O. Salvado, Symmetric diffeomorphic registration of fibre orientation distributions, Neuroimage. 56 (2011) 1171–1180, https://doi.org/10.1016/j.neuroimage.2011.02.014.
[26] D. Raffelt, J.-D. Tournier, S. Crozier, A. Connelly, O. Salvado, Reorientation of fiber orientation distributions using apodized point spread functions, Magn. Reson. Med. 67 (2012) 844–855, https://doi.org/10.1002/mrm.23058.
[27] Ca M. Wheeler-Kingshott, S. a Trip, M.R. Symms, G.J.M. Parker, G.J. Barker, D. H. Miller, In vivo diffusion tensor imaging of the human optic nerve: pilot study in normal controls, Magn. Reson. Med. 56 (2006) 446–451, https://doi.org/10.1002/mrm.20964.
[28] N. Gupta, L.-C. Ang, L. Noël de Tilly, L. Bidaisee, Y.H. Yücel, Human glaucoma and neural degeneration in intracranial optic nerve, lateral geniculate nucleus, and visual cortex, Br. J. Ophthalmol. 90 (2006) 674–678, https://doi.org/10.1136/bjo.2005.086769.
[29] Y.H. Yücel, N. Gupta, M.W. Kalichman, A.P. Mizisin, W. Hare, M. de Souza Lima, L. Zangwill, R.N. Weinreb, Relationship of optic disc topography to optic nerve fiber number in glaucoma, Arch. Ophthalmol. (Chicago, Ill. 1960) 116 (1998) 493–497, https://doi.org/10.1001/archopht.116.4.493.
[30] Y.H. Yücel, M.W. Kalichman, A.P. Mizisin, H.C. Powell, R.N. Weinreb, Histomorphometric analysis of optic nerve changes in experimental glaucoma, J. Glaucoma 8 (1999) 38–45, https://doi.org/10.1109/RE.2008.49.
[31] C.A.M. Wheeler-Kingshott, G.J.M. Parker, M.R. Symms, S.J. Hickman, P.S. Tofts, D. H. Miller, G.J. Barker, ADC mapping of the human optic nerve: increased resolution, coverage, and reliability with CSF-suppressed ZOOM-EPI, Magn. Reson. Med. 47 (2002) 24–31, https://doi.org/10.1002/mrm.10016.
[32] W.A. Lagrèze, M. Gaggl, M. Weigel, J. Schulte-Mönting, A. Bühler, M. Bach, R. D. Munk, T.A. Bley, Retrobulbar optic nerve diameter measured by high-speed magnetic resonance imaging as a biomarker for axonal loss in glaucomatous optic atrophy, Invest. Ophthalmol. Vis. Sci. 50 (2009) 4223–4228, https://doi.org/10.1167/iovs.08-2683.
[33] M.G. Ersoz, Y. Pekcevik, E. Ayintap, İ.B. Gunes, D.K. Mart, E. Yucel, G. Türe, MR imaging of the anterior visual pathway in primary open-angle Glaucoma: correlation with Octopus 101 perimetry and spectralis optical coherence tomography findings, Curr. Eye Res. 42 (2017) 995–1001, https://doi.org/10.1080/02713683.2017.1279633.
[34] R.L. Furlanetto, S.H. Teixeira, C.P.B. Gracitelli, C.L. Lottenberg, F. Emori, M. Michelan, E. Amaro, A. Paranhos, Structural and functional analyses of the optic nerve and lateral geniculate nucleus in glaucoma, PLoS One 13 (2018), e0194038, https://doi.org/10.1371/journal.pone.0194038.
[35] W.W. Chen, N. Wang, S. Cai, Z. Fang, M. Yu, Q. Wu, L. Tang, B. Guo, Y. Feng, J. B. Jonas, X. Chen, X. Liu, Q. Gong, Structural brain abnormalities in patients with primary open-angle glaucoma: a study with 3T MR imaging, Invest. Ophthalmol. Vis. Sci. 54 (2013) 545–554, https://doi.org/10.1167/iovs.12-9893.
[36] M. Fukuda, K. Omodaka, Y. Tatewaki, N. Himori, I. Matsudaira, K.M. Nishiguchi, T. Murata, Y. Taki, T. Nakazawa, Quantitative MRI evaluation of glaucomatous changes in the visual pathway, PLoS One 13 (2018), e0197027, https://doi.org/10.1371/journal.pone.0197027.
[37] L. Brun, A. Pron, J. Sein, C. Deruelle, O. Coulon, Diffusion MRI: Assessment of the Impact of Acquisition and Preprocessing Methods Using the BrainVISA-Diffuse Toolbox, Front. Neurosci. 13 (2019) 536, https://doi.org/10.3389/fnins.2019.00536.
[38] S. Haykal, B. Curcic-Blake, N.M. Jansonius, F.W. Cornelissen, Fixel-based analysis of visual pathway white matter in primary open-angle Glaucoma, Invest. Ophthalmol. Vis. Sci. 60 (2019) 3803–3812, https://doi.org/10.1167/iovs.19-27447.
[39] J.-C. Mwanza, D.L. Budenz, J.L. Warren, A.D. Webel, C.E. Reynolds, D.T. Barbosa, S. Lin, Retinal nerve fibre layer thickness floor and corresponding functional loss in glaucoma, Br. J. Ophthalmol. 99 (2015) 732–737, https://doi.org/10.1136/bjophthalmol-2014-305745.
[40] D.W. Lee, J.M. Kim, K.H. Park, C.Y. Choi, J.G. Cho, Effect of media opacity on retinal nerve fiber layer thickness measurements by optical coherence tomography, J. Ophthalmic Vis. Res. 5 (2010) 151–157. http://www.ncbi.nlm.nih.gov/pubmed/22737349.
[41] P. Venugopalan, Y. Wang, T. Nguyen, A. Huang, K.J. Muller, J.L. Goldberg, Transplanted neurons integrate into adult retinas and respond to light, Nat. Commun. 7 (2016), 10472, https://doi.org/10.1038/ncomms10472.
[42] D. Rusciano, S. Pezzino, M.G. Mutolo, R. Giannotti, A. Librando, N. Pescosolido, Neuroprotection in Glaucoma: old and new promising treatments, Adv. Pharmacol. Sci. 2017 (2017), 4320408, https://doi.org/10.1155/2017/4320408.
[43] P. Lu, L. Shi, H. Du, B. Xie, C. Li, S. Li, T. Liu, H. Feng, J. Wang, Reduced white matter integrity in primary open-angle glaucoma: a DTI study using tract-based spatial statistics, J. Neuroradiol. 40 (2013) 89–93, https://doi.org/10.1016/j.neurad.2012.04.001.
[44] M. Kaushik, S.L. Graham, C. Wang, A. Klistorner, A topographical relationship between visual field defects and optic radiation changes in glaucoma, Investig. Ophthalmol. Vis. Sci. 55 (2014) 5770–5775, https://doi.org/10.1167/iovs.14-14733.
[45] P. Frezzotti, A. Giorgio, I. Motolese, A. De Leucio, M. Iester, E. Motolese, A. Federico, N. De Stefano, Structural and functional brain changes beyond visual system in patients with advanced Glaucoma, PLoS One 9 (2014), e105931, https://doi.org/10.1371/journal.pone.0105931.
[46] W. Zhou, E.R. Muir, S. Chalfin, K.S. Nagi, T.Q. Duong, MRI study of the posterior visual pathways in primary open angle Glaucoma, J. Glaucoma 26 (2017) 173–181, https://doi.org/10.1097/IJG.0000000000000558.